Study of Geometry Effects on Heavy Atom Perturbation of the Electronic Properties of Derivatives of the Nonalternant Polycyclic Aromatic Hydrocarbons Fluoranthene and Acenaphtho[1,2-*k*]fluoranthene

Benjamin F. Plummer,* L. Kraig Steffen, Tala L. Braley, W. Greg Reese, Kathryn Zych, Gregory Van Dyke, and Brock Tulley

Contribution from the Department of Chemistry, Trinity University, San Antonio, Texas 78212-7200

Received July 28, 1993®

Abstract: A detailed study of the electronic behavior of a series of even nonalternant polycyclic aromatic hydrocarbons derived from fluoranthene is presented. Compounds were synthesized that contained substantial barriers to rotation of substituents into conjugation with the parent hydrocarbon. The heavy atom bromine was incorporated into several compounds to probe its ability to quench fluorescence by spin–orbital coupling. External heavy atom solvent effects on the quenching of fluorescence were also investigated. Fluorescence spectra are presented that clearly indicate that intramolecular heavy atom effects (HAEs) can be transmitted through phenyl substituents conjugated with a polycyclic aromatic hydrocarbon. The magnitude of the transmitted HAE is shown to vary as a function of the ability of the substituent to rotate into planarity with the polycyclic core. The steric strain present in the various fluoranthene derivatives is modeled using molecular mechanics and semiempirical molecular orbital calculations. Semiempirical molecular orbital calculations of the HOMO and LUMO energies are compared with data obtained experimentally by cyclic voltammetry.

Introduction

Cyclopentene-fused polycyclic aromatic hydrocarbons (CPAH) are a class of compounds that are related to the fullerenes which are constructed of fused hexagonal and pentagonal arrays of carbon atoms.[1-3] The reactivity of even, nonalternant CPAH is frequently different from even, alternant PAH.[4-6] When a benzenoid PAH is fused to a five-membered ring such as in fluoranthene (**2a**), steric strain results.[7] Recent studies on the nonalternant CPAH periflanthene (**4**) and 1,16-benzoperiflanthene[8] support the need for additional photophysical studies of fluoranthene derivatives.

The spectroscopic and electrochemical behavior of 7,10-disubstituted fluoranthenes, disubstituted 8,9-dihydrodiindeno-[1,2-*j*:2′,1′-*l*]fluoranthenes, and 7,14-disubstituted acenaphtho-[1,2-*k*]fluoranthenes are reported in this study. In several derivatives (Chart I) significant steric hindrance to the conjugation of substituents with the parent polycyclic nucleus is expected because of severe van der Waals overlap of nonbonded neighboring hydrogen atoms. X-ray crystallographic data clearly show that in the solid state the substituents are nearly perpendicular to the molecular plane of the CPAH in **1b**,[9] **1f**,[10] and **2b**.[9] This implies that 7,14-disubstituted **1b–f** should have a significantly decreased capacity for direct resonance of the substituents with the central

Chart I

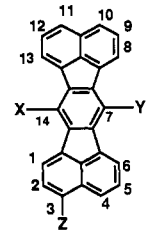

	X	Y	Z
1a	H	H	H
1b	Ph	Ph	H
1c	Ph	4-Cl Ph	H
1d	4-Cl Ph	4-Cl Ph	H
1e	4-Br Ph	4-Br Ph	H
1f	CO_2Et	CO_2Et	H
1g	Ph	Ph	Br

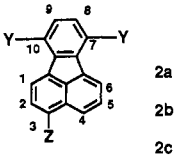

	Y	Z
2a	H	H
2b	Ph	H
2c	(4-BrPh)	H
2d	Ph	Br

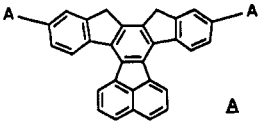

3a	H
3b	Br

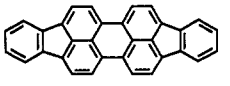

4

CPAH. The overlap integral Si,j (eq 1) between σ-bonded conjugated π systems is a function of the cosine of the dihedral.[11]

$$S_{i,j} = \beta \cos \theta \qquad (1)$$

As the dihedral moves from 90°, the overlap integral increases rapidly from 0 until the maximum value is reached at 0°. The

* Abstract published in *Advance ACS Abstracts,* November 1, 1993.

(1) Gao, Y.-D.; Herndon, W. C. *Mol. Phys.* **1992**, *77*, 585–599.
(2) Diederich, F.; Ettl, R.; Rubin, Y.; Whetten, R. L.; Marcos, R. B.; Anz, S.; Sensharma, D.; Wudl, F.; Khemani, K. C.; Koch, A. *Science* **1991**, *252*, 548–551.
(3) Curl, R. F.; Smalley, R. E. *Science* **1988**, *242*, 1017–1022.
(4) Dewar, M. J. S. *The Molecular Orbital Theory of Organic Chemistry*; McGraw-Hill: New York, 1969; pp 191–247.
(5) Plummer, B. F.; Singleton, S. F. *J. Phys. Chem.* **1989**, *93*, 5515.
(6) Plummer, B. F.; Singleton, S. F. *Tetrahedron Lett.* **1987**, *28*, 4801.
(7) Boyd, R. H.; Christensen, R. L.; Pua, R. *J. Am. Chem. Soc.* **1965**, *87*, 3554–3559.
(8) Schael, F.; Lohmannsroben, H.-G. *J. Photochem. Photobiol. A* **1992**, *69*, 27–32.
(9) Watson, W. H.; Kashyap, R. P.; Plummer, B. F.; Reese, W. G. *Acta Crystallogr.* **1991**, *C47*, 1848–1851.
(10) Plummer, B. F.; Reese, W. G.; Watson, W. H.; Kashyep, R. P. *Struct. Chem.* **1993**, *4*, 53–57.
(11) Streitwieser, A. J. *Molecular Orbital Theory for Organic Chemists*; Wiley: New York, 1962; pp 11–20.

0002-7863/93/1515-11542$04.00/0

absorption and emission spectra of these compounds were studied to see how their spectroscopic behavior would change as a function of the dihedral angle.

We also report the effect of heavy atoms on the photophysical properties of the fluoranthene derivatives. A halogen (Br, I) with high atomic number (heavy atom) attached directly to an aromatic compound can reduce significantly the fluorescence quantum yield.[12-16] The spin–orbit coupling mechanism of the heavy atom enhances the rate of intersystem crossing to the triplet state.[13,16,17] This is called the intramolecular heavy atom effect (HAE). Ethyl bromide and bromobenzene are solvents that contain heavy atoms, and they can also enhance intersystem crossing, giving rise to an intermolecular HAE.[18] The mechanism for the solvent heavy atom effect is complex and may involve the formation of weak charge-transfer complexes. Heavy atom effects are significantly influenced by the geometry of the heavy atom and the chromophore. In all three series of compounds studied here the relative position of the heavy atom–substituted phenyl group is such that it lies at the same distance and orientation with respect to the central polycyclic core. Using the HAE as a tool, we have explored the emission lifetime and quantum yields of fluorescence of the fluoranthene and acenaphtho[1,2-*k*]-fluoranthene derivatives as the dihedral angle is varied for the formally conjugated substituents. Molecular mechanics and semiempirical molecular orbital calculations are also used to probe the nature and extent of steric and substituent effects. Because the ease with which electrons can be added to or removed from the CPAH provides a direct measure of their reactivity, cyclic voltammetry was used to provide additional information about substituent effects. Equilibrium oxidation and reduction potentials ($E^{\circ\prime}$) were obtained to provide evidence for the relative stabilities of the cation and anion radicals, as measured by their reversible formation.

Experimental Section

General. ^{1}H NMR spectra were obtained on a Varian VXR-300 spectrometer at 300 MHz, using $CDCl_3$ solutions with internal tetramethylsilane (TMS). Melting points were determined on a Meltemp apparatus and are uncorrected. IR spectra were obtained as KBr pellets on a Perkin-Elmer 1600 FT-IR. Mass spectra were determined by direct insertion on a Hewlett-Packard 5995-C GC–mass spectrometer at 70-eV ionizing radiation. High-resolution mass spectra were determined by the Midwest Center for Mass Spectroscopy. Elemental analyses were performed by Texas Analytical Laboratories. Absorption spectra were obtained on a Cary 2315 UV/vis spectrophotometer. Samples were approximately 10^{-6} M in compound dissolved in spectral grade hexane or cyclohexane. A PTI model LS 100 spectrophotometer was used to determine emission lifetimes and steady-state fluorescence spectra.

Fluorescence Spectroscopy. Steady-state spectra were obtained on freshly prepared and argon-degassed solutions in spectral grade benzene or bromobenzene. Freshly prepared solutions of 9,10-diphenylanthracene (DPA) were used as references by adjusting absorbance values to about 0.2 AU at 381 nm, where all compounds showed significant absorption. The absorption of each compound in solution was adjusted to equal that of the standard DPA sample, and the fluorescence emission steady-state spectrum was obtained between 390 and 650 nm. The excitation, emission, and detector slits were set at 4, 2, and 4 nm, respectively. Fluorescence emisssion spectra were integrated, and the quantum yield was determined by the ratio of the integrated area to the integrated area of the fluorescence spectrum of DPA ($\Phi_F = 0.84$).[19] Excited-state lifetimes were measured on the same solutions used in the steady-state measurements. The excitation wavelength was set to 381 nm, and the emission wavelength was set to 470 or 480 nm. The slits were wide open.

Cyclic Voltammetry Oxidations. Voltammograms were measured at 25 °C on solutions approximately 10^{-3} M in compound and 0.1 M in tetrabutylammonium tetrafluoroborate supporting electrolyte. The solution used was a 8/1.5/0.5 mixture of methylene chloride/trifluoroacetic acid/trifluoroacetic anhydride.[20] The solvents were anhydrous reagent grade obtained from Aldrich and were used as obtained. Nitrogen gas was bubbled through the cell prior to running each cyclic voltammogram. A reference electrode Ag/0.1 M $AgNO_3$ in acetonitrile was used. The working electrode was a 0.05-cm^2 Pt disc and the counter electrode a Pt wire. Voltammetric data were collected at scan rates ranging from 10 to 1600 mV/s using a BAS Model 100A electrochemical system. Ferrocene was run as an internal redox standard, and its $E^{\circ\prime}$ is reported.

Reductions. Voltammograms were measured on solutions approximately 10^{-3} M in compound and 0.1 M in tetrabutylammonium tetrafluoroborate in anhydrous dimethylformamide. The supporting electrolyte and DMF were obtained from Aldrich and used as received. An aqueous Ag/AgCl reference electrode was used. Nitrogen gas was bubbled through the cell prior to determining each cyclic voltammogram. The counter and working electrodes were the same as those used for the oxidations.

Calculations. Molecular mechanics calculations were performed on a CACHE[21] system using MM2 parameters or with PCMODEL[22] using MMX. Dihedral calculations were geometry optimized at each fixed angle. Semiempirical molecular orbital calculations were performed using the MOPAC version of PM3[23] implemented on a Silicon Graphics IRIS personal workstation under SYBYL. Normal precision was used. All bonds and angles were geometry optimized. PM3 was chosen because it has performed well on related peri-fused polycyclic hydrocarbons.[24]

Synthesis. Purified fluoranthene was used as obtained from Aldrich. Compounds **1a**,[25] **2b**,[26,27] **1b**,[25] **1f**,[25] and **3a**[28] were synthesized according to literature procedures. Acecyclone and its substituted aryl derivatives were prepared according to literature procedures.[28,29]

7-(4-Chlorophenyl)-14-phenylacenaphtho[1,2-*k*]fluoranthene (1c). Into a 250-mL round-bottom flask fitted with a reflux condenser and magnetic stirrer containing a solution of 1-bromoacenaphthylene[30] (1.3 g, 5.5 mmol) and xylenes (25 mL) was added 4-(chlorophenyl)phenylacecyclone (2.0 g, 5.0 mmol), and the solution was refluxed for 52 h. When evolution of HBr was negligible, the solution was cooled to 0 °C and the yellow solid was collected by vacuum filtration. The solid was dissolved in 50% THF/methanol (300 mL) and the resulting green solution treated with $NaBH_4$ (0.2 g) to reduce unreacted cyclone. Addition of water (50 mL) caused the precipitation of a yellow solid (0.5 g, 19%) that was recrystallized from xylene: mp 343–346 °C; ^{1}H NMR ($CDCl_3$, 300 MHz) δ 7.65–7.78 (m, 12, ArH), 7.4 (dd, 1, J = 8.2, 7.2 Hz, H5), 7.37 (dd, 1, J = 8.2, 7.2 Hz, H2), 6.81 (d, 1, J = 7.2 Hz, H1), 6.76 (d, 1, J = 7.2 Hz, H6) δ = 7.76 (dd, 1, J = 8.5, 0.5 Hz, H3), 7.73 (d, 1, J = 8.1 Hz, H4), 7.63 (d, 1, J = 8.1 Hz), 7.39 (dd, 1, J = 8.1, 7.1 Hz), 6.74 (d, 1, J = 7.1 Hz). Anal. Calcd for $C_{38}H_{21}Cl$: C, 88.96; H, 4.13; Cl, 6.91. Found: C, 89.26; H, 4.15; Cl, 6.96.

7,14-Bis(4-chlorophenyl)acenaphtho[1,2-*k*]fluoranthene. (1d). Into a 100-mL round-bottom flask fitted with a reflux condenser and magnetic stirrer containing a solution of 1-bromoacenaphthylene (0.5 g, 1.9 mmol) and xylenes (25 mL) was added bis(4-chlorophenyl)acecyclone (0.7 g, 1.6 mmol), and the solution was refluxed for 24 h. When evolution of HBr was negligible, the solution was cooled and the xylenes removed by rotary evaporation. The tarry product was dissolved in 50% methylene chloride/cyclohexane (30 mL) and filtered through a layer of active alumina on a Buchner funnel. The filtrate was vacuum rotary evaporated to yield a yellow solid that was recrystallized from methylene chloride/cyclohexane (1/1) to yield 0.5 g of product (71%): mp dec > 350 °C;

(12) Lewitzka, F.; Lohmannsroben, H.-G. *J. Photochem. Photobiol. A* **1991**, *61*, 191–200.
(13) Cowan, D. O.; Drisko, R. L. *Elements of Organic Photochemistry*; Plenum: New York, 1976; pp 250–259.
(14) McGlynn, S. P.; Azumi, T.; Kinoshita, M. *Molecular Spectroscopy of the Triplet State*; Prentice Hall: Englewood Cliffs, NJ, 1969.
(15) Chandra, A. K.; Turro, N. J.; Lyoons, A. L.; Stone, P. *J. Am. Chem. Soc.* **1978**, *100*, 4964–4968.
(16) Robinson, G. W.; Frosch, R. P. *J. Chem. Phys.* **1962**, *38*, 1187.
(17) McClure, P. S. *J. Chem. Phys.* **1949**, *17*, 905.
(18) Kasha, M. J. *J. Chem. Phys.* **1952**, *20*, 72.
(19) *Handbook of Organic Photochemistry*; Wintgens, V., Ed.; CRC Press: Boca Raton, FL, 1989; Vol. 1, Chapter 17, Table I.
(20) Hammerich, O.; Parker, V. D. *J. Am. Chem. Soc.* **1974**, *93*, 4289.
(21) Tektronix In CACHE Manual, Beaverton, OR, 1992.
(22) Gilbert, K. E. Serena Software, Bloomington, IN.
(23) Stewart, J. J. P. *J. Comput.-Aided Mol. Des.* **1990**, *4*, 1.
(24) Plummer, B. F.; Steffen, L. K.; Herndon, W. H. *Struct. Chem.* **1993**, *4*, 279–285.
(25) Tucker, S. H. *J. Chem. Soc.* **1958**, 1462.
(26) Craig, J. T.; Robins, M. D. W. *Aust. J. Chem.* **1968**, *21*, 2237–2245.
(27) Abramov, V. S. *Dokl. Akad. Nauk SSSR* **1948**, *62*, 637.
(28) Dilthey, W.; Henkels, S. *J. Prakt. Chem.* **1937**, *85*, 85–97.
(29) Pascal, R. B.; McMillan, W. D.; Van Engen, D.; Eason, R. G. *J. Am. Chem. Soc.* **1987**, *109*, 4660–4665.
(30) Rice, J. E.; He, Z.-M. *J. Org. Chem.* **1990**, *55*, 5490–5494.

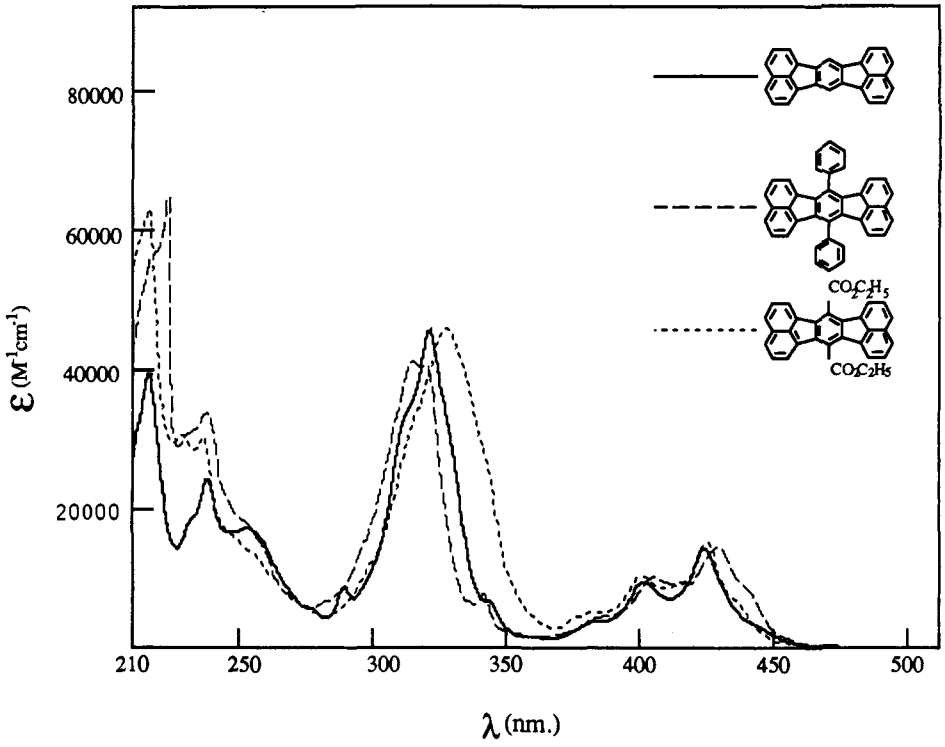

Figure 1. Absorption spectra of approximately 1×10^{-5} M solutions of **1a** (—), **1b** (- - -), and **1f** (– – –) in cyclohexane.

^{1}H NMR ($CDCl_3$, 300 MHz) δ 7.76 (dd, 1, J = 8.5, 0.5 Hz, H3), 7.73 (d, 1, J = 8.1 Hz, meta phenyl), 7.63 (d, 1, J = 8.1 Hz, ortho phenyl), 7.39 (dd, 1, J = 8.1, 7.1 Hz, H2), 6.74 (d, 1, J = 7.1 Hz, H1). Anal. Calcd for $C_{38}H_{20}Cl_2$: C, 83.36; H, 3.68; Cl, 12.95. Found: C, 83.59; H, 3.70; Cl, 12.85.

7,14-Di(4-bromophenyl)acenaphtho[1,2-*k*]fluoranthene (1e). Into a 100-mL round-bottom flask fitted with a reflux condenser and magnetic stirrer containing a solution of 1-bromoacenaphthylene (0.9 g, 3.8 mmol) and xylenes (25 mL) was added the brominated acecyclone (1.35 g, 2.62 mmol), and the solution was boiled at reflux for 2.5 days. After cooling overnight at 0 °C, insoluble acecyclone was removed by gravity filtration and the solid rinsed with warm xylenes (50 mL). The filtered xylene solution was concentrated by vacuum rotary evaporation and the resulting brown solid recrystallized from toluene to give yellow crystals (0.43 g, 26%): mp > 400 °C; ^{1}H NMR ($CDCl_3$, 300 MHz) δ 7.89 (d, 1, J = 8.3 Hz, meta phenyl), 7.78 (d, 1, J = 7.8 Hz, H3), 7.58 (d, 1, J = 8.3 Hz, ortho phenyl), 7.40 (dd, 1, J = 8.3, 7.2 Hz, H2), 6.79 (d, 1, J = 7.2 Hz, H1). Anal. Calcd for $C_{38}H_{20}Br_2$: C, 71.74; H, 3.14; Br, 25.12. Found: C, 71.48; H, 3.18; Br, 25.02.

3-Bromo-7,14-diphenylacenaphtho[1,2-*k*]fluoranthene (1g). Into a 100-mL round-bottom flask fitted with a reflux condenser and magnetic stirrer containing a solution of 1,5-dibromoacenaphthylene (0.50 g, 1.59 mmol) in xylenes (60 mL) was added diphenylacecyclone (0.52 g, 1.4 mmol), and the solution was refluxed for 72 h, at which time the evolution of HBr was negligible. The solution was cooled to 0 °C and the unreacted cyclone removed by gravity filtration. The solution was vacuum rotary evaporated, giving a brownish yellow solid that upon recrystallization from toluene produced yellow crystals (0.28 g, 36%): mp 316–318 dec; ^{1}H NMR ($CDCl_3$, 300 MHz) δ 6.5 (d, 1H, J = 7.6 Hz), 6.73 (m, 3H), 7.18 (bs, 1H, J = 7.4 Hz), 7.32 (d, 1H, J = 7.2 Hz), 7.35 (d, 1H, J = 7.1 Hz), 7.39 (dd, 1H, J = 8.4, 7.2 Hz), 7.56 (d, 1H, J = 7.6 Hz), 7.7 (m, 11H), 7.89 (d, 1H, J = 8.2 Hz); HRMS Calcd for $C_{38}H_{21}{}^{81}Br$, 558.0807; found, 558.0812.

7,10-Di(4-bromophenyl)fluoranthene (2c). A solution of di(4-bromophenyl)acecyclone (1.10 g, 21 mmol) in 75 mL of norbornadiene in a 100-mL round-bottom flask fitted with a reflux condenser, nitrogen purging, and a magnetic stirrer was refluxed for 24 h. The excess norbornadiene was removed by simple distillation and vacuum rotary evaporation to give a gray solid. The solid was dissolved in hot toluene, treated with charcoal, and cooled to produce yellow-green crystals (0.3 g): mp 312–314 °C; ^{1}H NMR ($CDCl_3$, 300 MHz) δ 7.21 (s, 1H), 7.26 (d, 1H, J = 7.3 Hz), 7.39 (d, 1H, J = 7.1), 7.42 (d, 1H, J = 7.2 Hz), 7.52 (d, 1H, J = 8.4 Hz), 7.69 (d, 1H, J = 8.4 Hz), 7.79 (d, 1H, J = 7.6 Hz); HRMS Calcd for $C_{28}H_{16}{}^{81}Br_2$, 513.9579; found, 513.9582.

3-Bromo-7,10-diphenylfluoranthene. (2d) Into a 100-mL round-bottom flask fitted with a reflux condenser and magnetic stirrer were added 7,10-diphenylfluoranthene (**2b**) (1.01 g, 2.85 mmol), DMF (50 mL), and *N*-bromosuccinimide (1.01 g, 5.68 mmol).[31] After refluxing for 1.5 h, TLC indicated the prescence of starting material. More NBS (1.18 g, 6.23 mmol) was added and the solution refluxed overnight. The solvent was removed by vacuum rotary evaporation and the residue dissolved in methylene chloride, extracted with dilute HCl, dried over $MgSO_4$, and filtered. After removal of the solvent, the crude solid (0.45 g) was subjected to column chromatography (silica, hexanes). A pale yellow solid was isolated and recrystallized from absolute ethanol to give **2d** (0.12 g, 10%): mp 115–117 °C; ^{1}H NMR ($CDCl_3$, 300 MHz) δ 7.04 (d, 1H, J = 7.63 Hz), 7.23 (d, 1H, J = 7.1 Hz), 7.30 (s, 2H), 7.44 (m, 1H), 7.61 (m, 11H), 7.95 (d, 1H, J = 8.5 Hz); HRMS Calcd for $C_{28}H_{17}{}^{81}Br$, 434.0494; found, 434.0481.

9,14-Dibromo-8,9-dihydroindeno[1,2-*j*:2′,1′-*l*]-11,12-dioxofluoranthene (used to prepare 3b). Anhydrous aluminum chloride (6.70 g, 0.05 mol) and sodium chloride (1.46 g, 0.025 mol) were placed in a two-neck 250-mL round-bottom flask that was lightly stoppered with aluminum foil-wrapped rubber stoppers, fitted with a thermometer, and heated to 180 °C. Powdered 9,10-bis(4-bromophenyl)-8,9-fluoranthenedicarboxylic acid anhydride (3.0 g, 5.15 mmol) was added slowly over a period of about 1.5 h with stirring, while maintaining the temperature at 180 °C, and then the cooled reaction mixture was quenched with concentrated HCl (50 mL) in ice (300 g). The mixture was then poured into ice and water (400 g) in a 500-mL beaker and the dark precipitate collected by vacuum filtration. The dark solid was washed with distilled water (50 mL) to yield a black solid, which was extracted for 20 h with xylenes (300 mL) using Soxhlet extraction. A deep red solution was obtained, which upon cooling yielded deep red crystals of diketone (1.48 g, 51%): mp > 400 °C; IR (KBr) 3205, 1725 (C=O), 1588, 1567, 1456, 1417, 1375, 1319, 1267, 1255, 1208, 1173, 1112, 1063, 896, 816 cm^{-1}.

9,14-Dibromo-8,9-dihydrodiindeno[1,2-*j*: 2′,1′-*l*] fluoranthene (3b). Granular zinc (20 g, 0.306 mol) was added to a 250-mL round-bottom flask with concentrated HCl (5 mL) and mercuric chloride (10 g, 0.037 mol) and stirred for 5 min, and the liquid was decanted. A solution of diketone (1.3 g, 2.3 mmol) in xylenes (100 mL) and 7 M HCl (35 mL) was added and refluxed for 25 h, during which time the solution became yellow-orange. The heterogeneous mixture was cooled and extracted with ethyl ether (4 × 100 mL), and the combined organic phase was washed with KOH (50% by wt, 2 × 25 mL) and saturated $NaHCO_3$ (3

(31) Ross, S. D.; Finkelstein, M.; Peterson, R. C. *J. Am. Chem. Soc.* **1958**, *80*, 4327–4330.

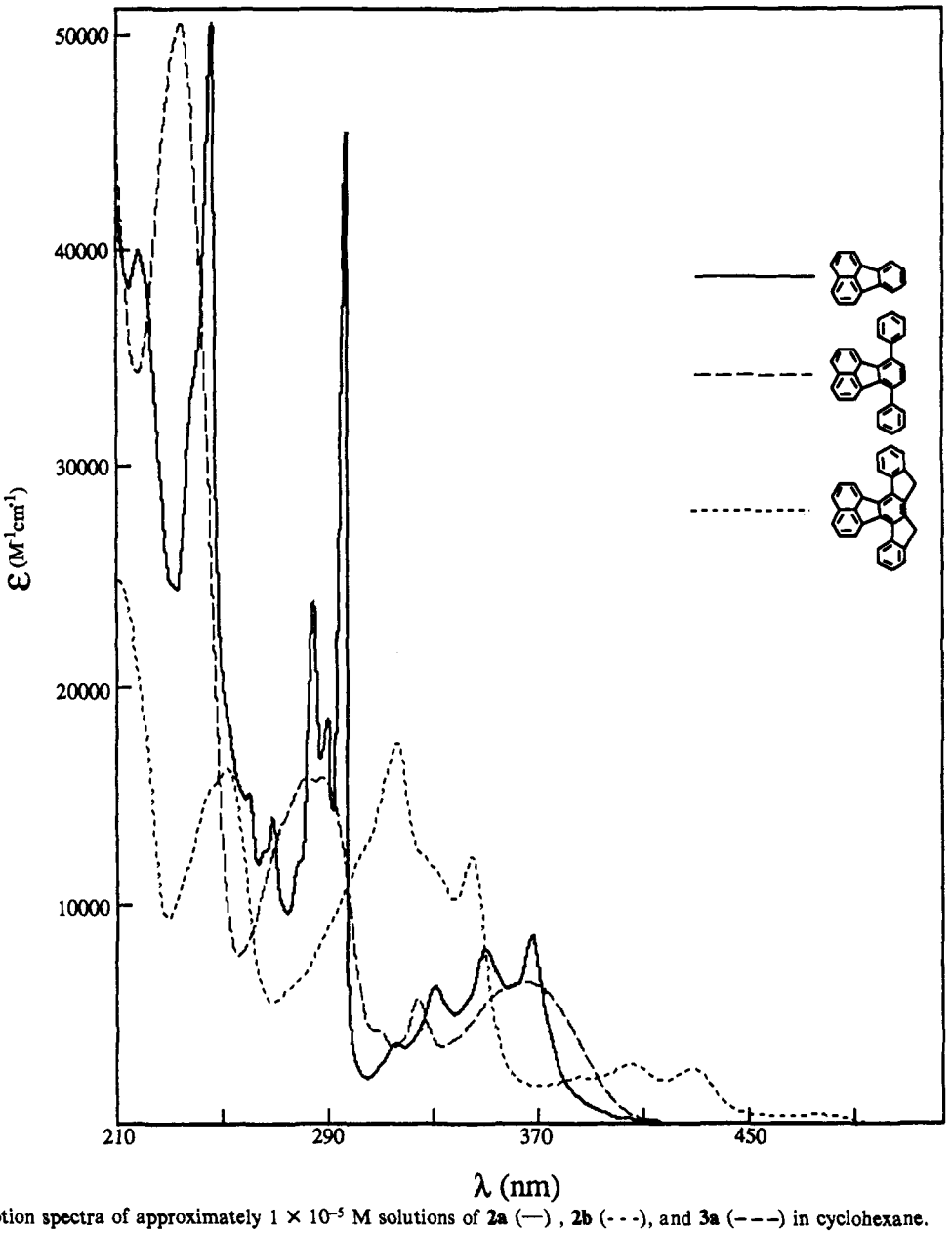

Figure 2. Absorption spectra of approximately 1×10^{-5} M solutions of **2a** (—), **2b** (- - -), and **3a** (– – –) in cyclohexane.

× 25 mL) and dried (Na_2SO_4). The combined organic phase was vacuum rotary evaporated and a yellow-brown solid formed. The crude product was purified by washing with warm ether to give a yellow-orange solid (0.22 g, 17%). After recrystallization from ether/methanol, it had a mp of 298 °C dec; IR (KBr) 1686, 1654, 1637, 1560, 1458, 1399, 1331, 1071, 920, 766 cm^{-1}; ^1H NMR ($CDCl_3$, 300 MHz) δ 3.95 (s, 2H), 7.61 (dd, 1H, J = 2.0, 8.6 Hz), 7.71–7.78 (m, 2H, broad s superimposed upon a dd), 7.92 (d, 1H, J = 8.2 Hz), 8.48 (d, 1H, J = 8.2 Hz), 8.59 (d, 1H, J = 7.0 Hz). Anal. Calcd for $C_{30}H_{16}Br_2$: C, 67.19; H, 3.01; Br, 29.80. Found: 66.94, 2.88, 29.92.

Results and Discussion

Absorption Spectra. The absorption spectra of the 7,14-disubstituted (**1a-g**) and 7,10-disubstituted (**2a-c**) derivatives within each series of compounds exhibited small perturbations from the parent hydrocarbon (Figure 1). The small red shift observed in the long wavelength bands for **1b** compared to those for **1a** may result from a small amount of conjugation of the substituents (vide infra). A detailed study of the linear dichroism spectra of **1a**, **1b**, and **1f** has shown that the most intense bands are long axis polarized.[32] Compound **2b** shows a slight blue shift in comparison to **2a**. Further solvent studies are required to determine the origin of this perturbation. Compound **3** exhibits a large (50 nm) red shift for the lowest energy bands compared to **2a**, reflecting the fact that in-plane conjugation of the phenyl substituents has a significant effect on the absorption spectrum (Figure 2). The absorption spectra show measurable differences at wavelengths beginning around 230 nm. For compounds substituted by phenyl substituents, enhanced absorption in this region is probably the result of local excited states in which the benzene chromophore undergoes excitation into its intense band ($^1B_{1u}$) typically found near 210 nm.[33]

Emission Spectra. In the absence of photochemistry the fluorescence quantum yield Φ_F of an emitting substance is given by the ratio of rate constants shown in eq 2.

$$\Phi_F = k_F/(k_F + k_{ISC} + k_{IC}) = k_F\tau_F = \tau_F/\tau_0 \qquad (2)$$

The subscripts denote respectively the processes of fluorescence (F), intersystem crossing (ISC), and internal conversion (IC). The parameters τ_F and τ_0 represent respectively the fluorescence and radiative lifetimes. In the presence of a heavy atom such as

(32) Plummer, B. F. Unpublished observations.

(33) Jaffe, H. H.; Orchin, M. *Theory and Applications of Ultraviolet Spectroscopy*; Wiley: New York, 1962.

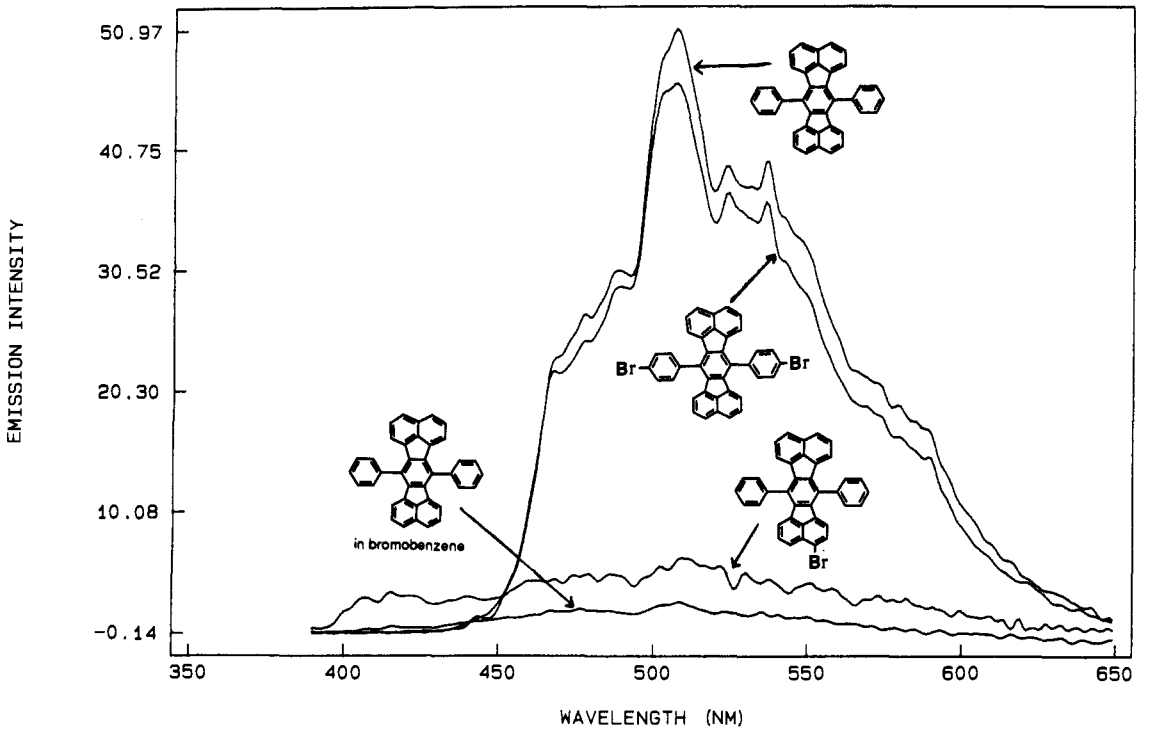

Figure 3. Fluorescence emission spectra of **1b**, **1e**, and **1g** in benzene and **1b** in bromobenzene. λ_{ex} = 381 nm (N_2 arc); $A \approx 0.2$ au. Intensities were normalized with respect to a 9,10-diphenylanthracene standard, and the integrated areas under the curves are proportional to the quantum yield.

bromine or iodine the rate constant k_{ISC} is increased, and hence both τ_F and Φ_F are reduced significantly as k_{ISC} grows larger.

The steady-state fluorescence emission spectra of most of the compounds were obtained in benzene and bromobenzene. The spectra exhibit similarity in shape and fine structure through each series of related structures. The emission of the acenaphtho-[1,2-*k*]fluoranthene derivatives **1a-g** typically gave broad bands from 440 to 650 nm, with maxima near 510 nm. The 7,10-disubstituted fluoranthenes also gave a broad emission band and exhibited maxima at around 460 nm. The intensity of the fluorescence emission of individual compounds changes considerably as a function of substituents and solvent used. The values obtained for Φ_F (Table II) were standardized relative to the literature value reported for 9,10-diphenylanthracene (Φ_F = 0.84).[19] Fluorescence lifetimes were also measured in benzene and bromobenzene and fluorescence rate constants determined from the lifetimes and quantum yields. The emission spectra of **1b**, **1e**, and **1g** in benzene and **1b** in bromobenzene (Figure 3) are shown on a normalized plot. The qualitative shape of the emission curves is very similar in benzene and bromobenzene, but the intensity relative to the benzene data has decreased significantly. The bis(4-bromophenyl) substituted compound, **1e**, produces a small reduction of about 10% in Φ_F. This small perturbation indicates that the intramolecular heavy atom quenching of fluorescence by the bromines is very inefficient. This result contrasts sharply with the profound HAE on the fluorescence of **1g**, which has the bromine substituent covalently bonded to the CPAH core. The bromobenzene solvent quenches the fluorescence of most of the compounds very effectively, with a decrease in fluorescence quantum yield of greater than 85% relative to the data obtained in benzene. The overall quantum yield for **1e** and **1g** is lower than that for **1b** in bromobenzene, indicating that fluorescence quenching occurs through both the inter- and intramolecular HAE.

The fluorescence of the 7,10-disubstituted fluoranthene derivatives is also quenched in a similar way (Table II). The 4-bromophenyl substituents in **2c** can rotate more freely (vide infra) than the same substituents in **1b**, and accordingly **2c** shows a 77% decrease in Φ_F compared to **2b**. When this result is compared to the HAE found for **1e**, it is obvious that a much stronger intramolecular heavy atom perturbation occurs in the series **2** derivatives (Figure 4). Compounds **1g** and **2d** were synthesized in order to compare the intramolecular quenching that results from covalent bonding of a heavy atom to the polycyclic aromatic core. Similar to the results obtained for **1g**, **2d** shows a very strong HAE. As anticipated, the brominated product **2c** exhibits an even lower quantum yield in bromobenzene than **2b**. The combination of internal and external heavy atom perturbation is larger than the sum of the individual effects.[14]

An even more dramatic HAE is seen when the results for **3a** and **3b** are compared (Figure 5). The substituted phenyl groups are bridged with fused methylene groups, forcing the entire molecular structure to adopt a near planar geometry. The corresponding dihedral angle for the conjugated coplanar phenyl is computed to be about 15°. Because of the cos θ relationship between the dihedral angle and the overlap integral, conjugation between phenyl and the fluoranthene parent is greatly increased. Compound **3b** has bromine substituents bonded to the phenyl groups that are nearly coplanar with the fluoranthene nucleus. The data show that Φ_F is very small and that the intramolecular HAE in **3b** is a very large perturbation. Parent **3a** also produces intriguing results. When the values of Φ_F for **3a** measured in benzene and bromobenzene are compared, the observed decrease in Φ_F attributable to the external HAE is only 70%. The lesser degree of external heavy atom quenching for series **3** compounds compared to the other compounds requires further inquiry as to the rationale for this behavior.

Only one phosphorescence experiment was performed. Preliminary results showed no phosphorescence emission for **1b** in frozen, degassed 3-methylpentane at −77 °C.

Fluorescence Lifetimes. In benzene, **3a** and **3b** exhibited transients whose measured lifetimes could only be fitted by a biexponential curve. These results may be due to the inherent strain in the system inducing local excited states to occur. The observed τ_F values for all compounds studied decrease significantly as the solvent is changed from benzene to bromobenzene. For **1b** in benzene and in bromobenzene, respectively, τ_F = 23.1 ns and decreases to τ_F = 2.4 ns. Representative fluorescence decays are shown for **1b** in benzene and in bromobenzene (Figure 6). The very short lifetimes observed in bromobenzene are near the

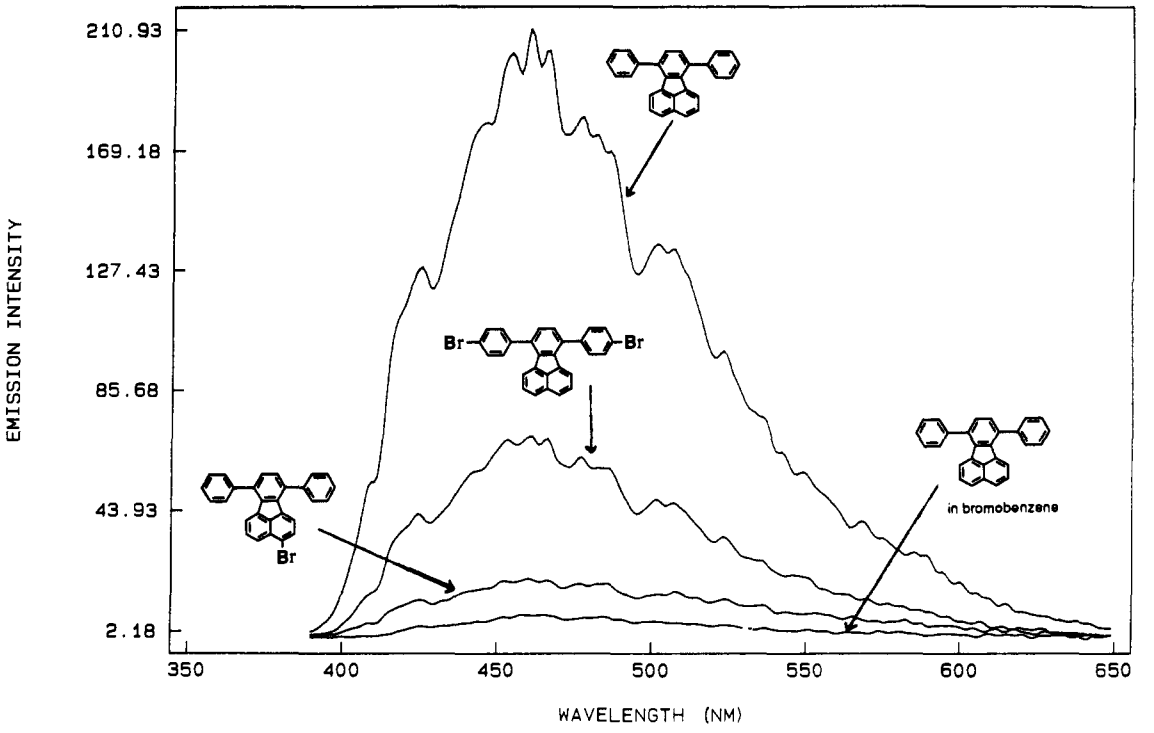

Figure 4. Fluorescence emission spectra of **2b**, **2c**, and **2d** in benzene and **2b** in bromobenzene (see caption for Figure 3).

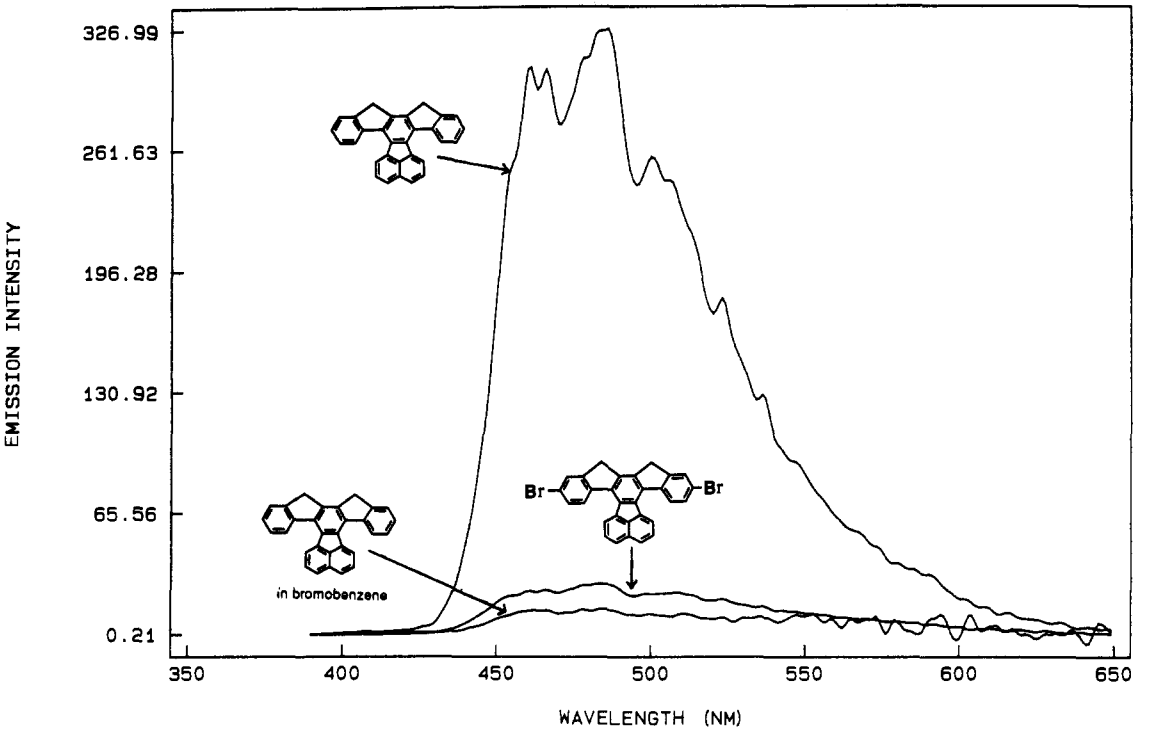

Figure 5. Fluorescence emission spectra of **3a** and **3b** in benzene and **3a** in bromobenzene (see caption for Figure 3).

limits of resolution of our instrument and are less accurate. Interesting solvent effects are observed. For the acenaphtho[1,2-*k*]fluoranthene series the values of the rate constant k_f decrease in magnitude when benzene is compared to bromobenzene. The 7,10-diphenylfluoranthene series shows the opposite effect. The value of k_f increases in bromobenzene when compared with the value in benzene. Because the quantum yields in bromobenzene are very low, it is probable that experimental error is large enough to vitiate any small trends in the data.

The observed decreases in the fluorescence lifetimes for the brominated compounds are consistent with the quantum yield results. The lifetimes vary predictably for **1e**, **2c**, and **3b** (Table I) as a function of the dihedral angle subtended by the bromophenyl groups with respect to the central CPAH. The lifetime for **2a** is reported to be about 50 ns.[34] None of the compounds studied in this report show lifetimes nearly as long as that of **2a**. Compound **1e** gave a measured lifetime slightly less than that of **1b**, but this could be attributed to the experimental error in the measurement.

Structural Analysis. The steric interaction between the buttressing hydrogens of the central CPAH and the attached phenyl substituents was modeled by molecular mechanics. The

(34) Berlman, I. B. *Handbook of Fluorescence Spectra of Aromatic Molecules*; Academic Press: New York, 1971.

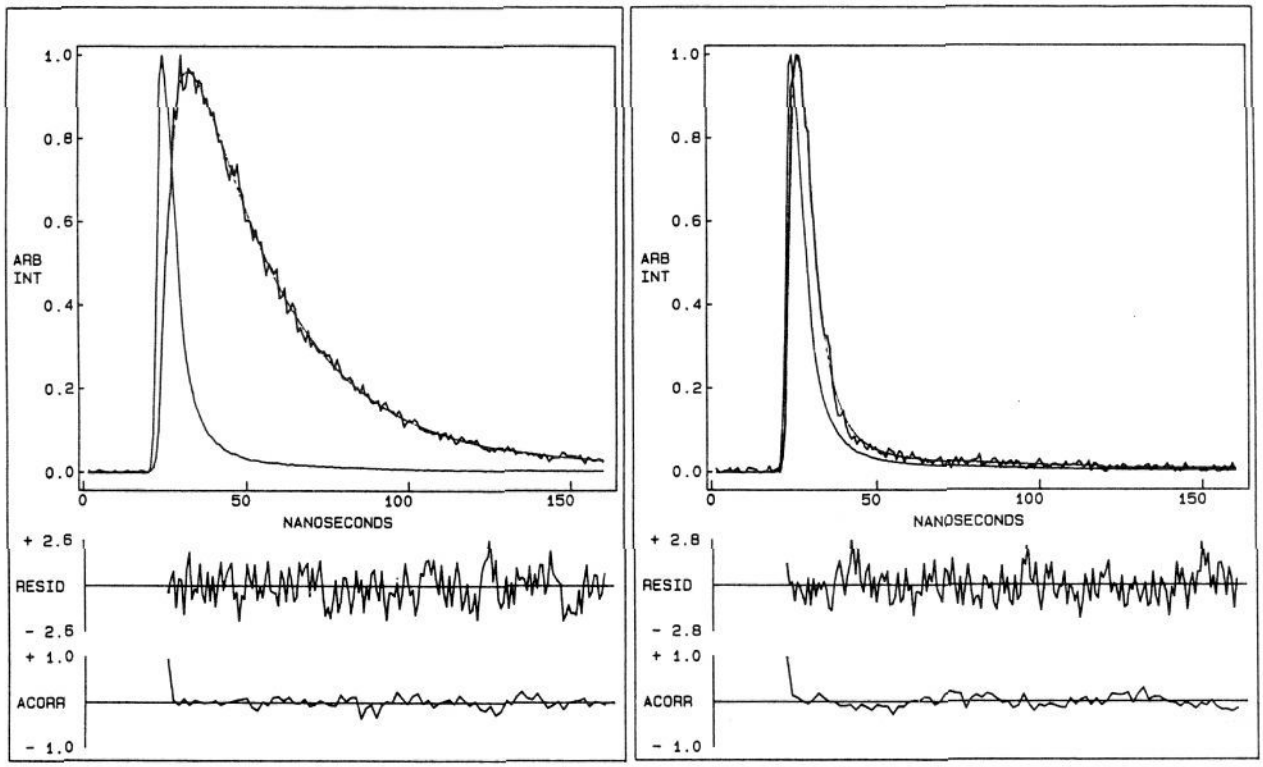

Figure 6. Fluorescence decay curve for **1b** in benzene (left) and in bromobenzene (right). λ_{ex} = 381 nm (N_2 arc); λ_{em} = 480 nm. The curves were fit by a single-exponential function with τ = 23 and 2.4 ns, respectively.

Table I. Fluorescence Spectroscopy of Fluoranthene Derivatives

	τ (ns)		Φ (DPA = 0.84)		k_F ($=\Phi/\tau \times 10^9$ s^{-1})	
compd	Bz[a]	BrBz[b]	Bz	BrBz	Bz	BrBz
DPA[c]	7.1		0.84		0.118	
1b	23	2.4	0.60	0.027	0.026	0.011
1e	23	1.5	0.54	0.024	0.024	0.016
1f	24	1.3	0.28	0.013	0.012	0.0098
1g	1.0[d]	1.7	0.028	0.017	0.028	0.010
2b	34	2.6	0.48	0.054	0.014	0.021
2c	8.3	2.6	0.16	0.034	0.019	0.021
2d	1.3	1.0	0.011	0.014	0.0082	0.014
3a	7.9[e]	2.1	0.50	0.10	0.053	0.047
3b	1.6[e]	1.0[f]	0.10	0.058	0.058	0.058

[a] Benzene. [b] Bromobenzene. [c] 9,10-Diphenylanthracene. [d] The fit for this decay was slightly better if a two-exponential fit was used, with the second component having τ = 11 ns. [e] A two-exponential decay was needed to fit the observed signal, with the minor component having a τ of 1.0 ns for **3a** and 9.8 ns for **3b**. [f] The fit was poor with a single or double exponential.

dihedral angle is defined as 0° when the substituent is in-plane and 90° when the substituent is perpendicular to the plane. The potential energy curve for **1b** shown in Figure 7 was obtained by computing at 5° increments the conformational energy that resulted as one phenyl–CPAH dihedral rotated while the rest of the molecule including the other phenyl substituent was allowed to optimize its geometry. A single potential energy minimum at a dihedral angle of 90° is computed. The cumulative steric effect of the nonbonded buttressing hydrogens on the rotation of the phenyl dihedral is sufficient to overcome any decrease in potential energy due to increased conjugation by the phenyl group as it moves toward coplanarity with the central core. As the dihedral angle for the σ-bonded phenyl substituent moves from 90° toward 0° the rest of the CPAH twists symmetrically, while the phenyl on the opposite side twists symmetrically in the reverse direction. The barrier for complete rotation of the phenyl substituent through the polycyclic plane was calculated to be about 20 kcal. A space-filling model of **1b** illustrates the significant van der Waals interactions that are present in these compounds.

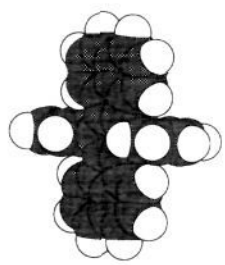

1b

A similar potential energy calculation performed on **2b**, which has two buttressing hydrogens instead of the four found in **1b**, shows two shallow potential minima at dihedral angles of 70° and 110°. The central barrier is very small, less than 0.5 kcal. Clearly, the phenyl substituent(s) in **2b** can rotate much more freely around the phenyl–CPAH σ-bond than they can in **1b**. The minimum energy conformation contains a small contribution due to conjugative interaction through resonance of the phenyl substituents with the polycyclic nucleus. Even at a dihedral of 30°, the computed potential energy in **2b** has increased to only 3.5 kcal above the minimum energy. The relative ease with which the phenyl substituents in **2b** can rotate past the buttressing hydrogens is due to the fact that the phenyl groups can effect an out-of-plane angle deformation as they rotate. The 21-kcal magnitude of the barrier for complete rotation of the phenyl substituents in **2b** is similar to that computed for **1b**. The accuracy of the magnitude of this calculated barrier remains to be tested.

Because the central portion of both **1b** and **2b** constitutes a *p*-terphenyl system, we have included the plot of its rotational energy. The energy minimum for each structure is arbitrarily adjusted so that the minima are set to 0 (Figure 7). The rotational barriers in *p*-terphenyl represent the minimal amount of steric

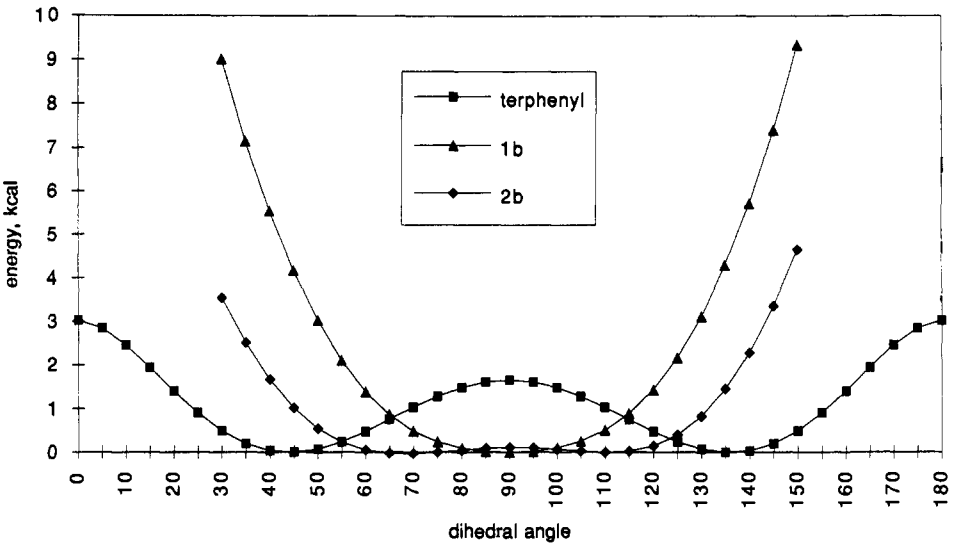

Figure 7. Molecular mechanics (CACHE) dihedral energy calculations for **1b**, **2b**, and *p*-terphenyl. Data were computed at 5° rotational increments, with full geometry optimization for all atoms being used except for the four fixed dihedral atoms.

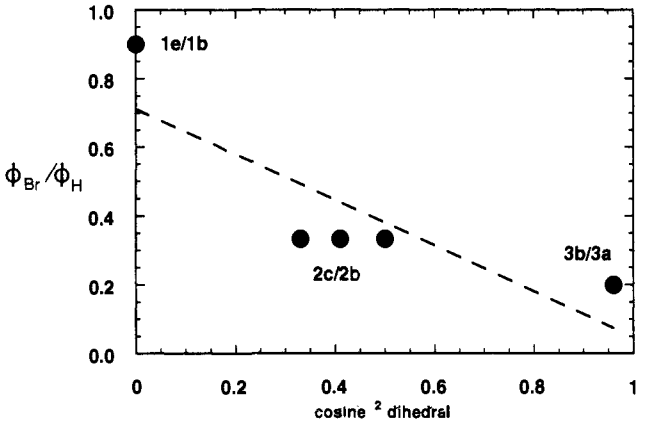

Figure 8. Correlation between the (cosine)^2 of the dihedral angle of the phenyl substituents and the central CPAH with the ratio of the quantum yields **1e/1b**, **2c/2b**, and **3b/3a**.

strain expected for rotation about the σ-bonded phenyl–CPAH core in the absence of buttressing hydrogens of the type present in **1b** and **2b**. The greater resonance stabilization available to the less sterically constrained terphenyl is clearly seen in the energy curves as the energy minima move closer to a dihedral of 0°.

The barriers computed for achieving in-plane conjugation generally agree with the fluorescence emission observations. The less sterically inhibited bromophenyl rotation possible in **2c** leads to a much greater intramolecular heavy atom effect than the highly constrained substituents in **1e**. It is assumed that the bromine substituents have an insignificant effect on the potential energy barriers illustrated by the dihedral energy curves. If the intramolecular HAE for the attached bromophenyl substituents follows the normal cos θ relationship for conjugation, then **3b** should be quenched significantly, **2c** should be quenched moderately, and **1e** should show only a small decrease due to the HAE. A plot of the (cosine)^2 of the dihedral angle obtained from the ground-state molecular mechanics calculations versus the ratio of the quantum yields for brominated and unbrominated phenyl substituents on **1**, **2**, and **3** yields a reasonable correlation (Figure 8). Because of the relatively soft barrier that exists for rotation of the phenyl substituents in **2b**, angles of 45°, 55°, and 65° are plotted for the **2c/2b** quantum ratio. These results indicate that the intramolecular HAE of covalently bonded bromine can be transmitted through an attached phenyl group when partial conjugation with the central CPAH occurs. It must be that the spin–orbital coupling matrix element between the phenyl ring and the polynuclear aromatic contains information imparted via the intramolecular spin–orbital coupling matrix element between the heavy atom and the phenyl ring.

Modeling van der Waals Strain. Is there more steric strain in **1b** or in **2c** when each adopts the minimum energy conformation? One measure of this energy difference is the VDW strain computed from the molecular mechanics calculations. A VDW strain of 10.3 and 13.0 kcal was computed for **2b** and **1b**, respectively. Terphenyl, the best model for the central part of the molecules with none of the long-range VDW interactions from buttressing hydrogens, has a VDW strain of 8.5 kcal. Semi-empirical (PM3)[23] calculations were also used to estimate the extra strain present. Geometry-optimized structures were obtained for selected compounds and heats of formation computed. These heats of formation were then compared to closely related structural isomers in which the 7,10 or 7,14 substituents were positioned on the perimeter of the CPAH to relieve all but biphenyl type interactions.

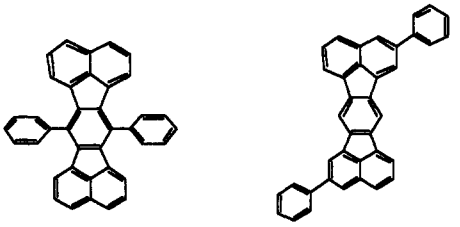

1b: H_f =192.4 2,9 isomer: H_f = 186.5

These structural isomers constitute idealized isodesmic interconversions, and although the absolute value of the heat of formation may not be particularly accurate, the relative energy difference should reflect any extra strain due to the extra VDW interactions present. Similar calculations on 7,10-diphenylfluoranthene and its related 2,5-diphenyl isomer gave heats of formation of 132.3 and 130.2 kcal/mol, respectively. More strain energy is present in **1b** compared with that in **2b**, as determined by this method, and the results are similar in magnitude to those obtained via molecular mechanics.

HOMO and LUMO energies and MO wave functions were also obtained from the PM3 calculations. For the **1a-e** series all of the HOMO's are located primarily on the central CPAH and consist mostly of π-type overlap of the fused rings (Figure 9). There is a small contribution to the HOMO by the overlap of the p-orbital component of the σ sp^2 hybrid orbitals of the attached phenyls. This unusual overlap appears to be due to the restricted

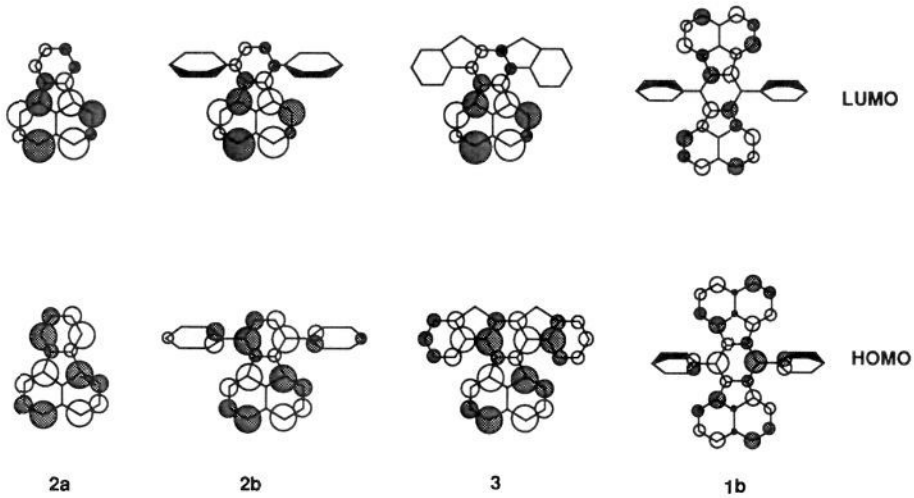

Figure 9. HOMO and LUMO diagrams (PM3) for compounds **1b**, **2a**, **2b**, and **3a**. The radii of the circles are drawn proportional to the magnitude of the AO at each atom.

Table II. Electrochemical and Calculated Molecular Orbital Energies

compd	E_{pa}(V)[a]	$E^{\circ\prime}_{ox}$	E_{pc}(V)[b]	$E^{\circ\prime}_{red}$	HOMO[c]	LUMO[c]
1a	1.060	1.020	−1.5131	−1.457	−8.698	−1.397
1b	1.119	1.079	−1.655	−1.609	−8.384	−1.378
1c			−1.398	−1.368		−1.240
1d	1.169	1.119	−1.375	−1.339	−8.505	−1.448
1e	1.203	1.150	−1.710	−1.670	−8.540	−1.480
1f	1.426	irrev	−1.269/−1.452	−1.218/−1.417	−8.365	−1.474
2a	1.360	irrev	−1.730	−1.680	−8.698	−1.061
2b	1.238	irrev	−1.641	−1.610	−8.633	−1.011
3a	0.933	0.891	−1.616	−1.570	−8.254	−1.074
ferrocene		0.080				

[a] Volts vs Ag/0.1 M $AgNO_3$ in CH_3CN. [b] Volts vs Ag/AgCl (aq). [c] Calculated using the program PM3.

rotation of the phenyls. The size of the coefficient for this overlap increases slightly as the substituent at the 4 position on the phenyl is changed from a hydrogen to chlorine, and to bromine, indicating a small inductive effect. The LUMO's for the **1a-e** series all have nodes at the 7,14 positions, and the wavefunctions were essentially unchanged by the substituents. The HOMO of **2b** has an increased contribution from the attached phenyls, and according to the calculation, it represents a mixture of the p-type σ overlap seen for the **1a-e** series and conventional π overlap. In **3a**, where the phenyls are forced into near planarity, the π overlap is increased significantly and the HOMO is spread over the entire molecule. These MO results are in accord with the findings presented earlier. For example, the increased contribution to the HOMO for **3** is evident in the UV/vis spectrum as a pronounced red shift. The increased overlap seen for **3b** and **2c** versus **1e** is reflected in the increased intramolecular heavy atom effect seen in **2c** and **3b**.

Cyclic Voltammetry Oxidations. Oxidation peak potentials (E_{pa}) are given and $E^{\circ\prime}$ values are shown for those compounds that exhibited reversible oxidation (Table II). The mixed solvent system of methylene chloride/trifluoroacetic acid/trifluoroacetic anhydride was shown to be an excellent solvent for generation of cationic species.[20] Trace amounts of water, which can react with cation radicals, are scavenged effectively by this mixture, and the cation radicals formed may also be stabilized by ion pair interactions with the trifluoroacetate. After correcting for differences in the reference electrode and comparing the data available for **2a** and anthracene,[35] it is apparent that in this solvent system the E_{pa} values are shifted anodically about 160 mV. This does not affect the conclusions derived from this study because relative oxidation potentials are compared. Reversibility was judged by a number of criteria. At 100 mV/s the ratio of the anodic and cathodic peak currents was close to or equal to 1. The peak potential shifted less than 20 mV as the scan rate was increased from 20 to 800 mV/s. The separation between the anodic and cathodic peaks was 80–110 mV. While the occurrence of a chemical reaction cannot be dismissed, it is probably due to the low polarity solvent used. All of the compounds produced diffusion-controlled oxidations, as indicated by linear plots of the square root of the sweep rate versus the anodic peak current. The trend observed for the **1a-f** series of small increases in the oxidation potential as the substituents are changed from H to phenyl to 4-chlorophenyl to 4-bromophenyl and finally to the diester is consistent with an inductive effect. The decreasing oxidation potential seen for **2a,b** and **3a** is a reflection of increased conjugation possible for **2a,b** and **3a**. The HOMO energies show similar trends with very closely related compounds such as **1b-e** but vary in a less predictable way between sets of compounds. (**1f** is harder to oxidize than **1b-d**, yet the HOMO is higher in energy, for example.) The reversibility of the oxidation of **3** versus the irreversibility of **2a** and **2b** is likely the result of ground-state destabilization of **3** due to increased steric strain coupled with the extra resonance stabilization available in **3** and $\mathbf{3}^{\cdot+}$. Molecular modeling shows no significant change in the geometry of **3** between the neutral and charged species. However, as is apparent from the MO diagrams (Figure 9), the calculations clearly show the extra stabilization available to **3** and likewise to $\mathbf{3}^{\cdot+}$ via resonance with the attached phenyl groups forced to become nearly coplanar with the fluoranthene nucleus.

Cyclic Voltammetry Reductions. All of the compounds studied showed reversible reductions, so $E^{\circ\prime}$ values are reported in addition to the E_{pc} values (Table II). The criterion for reversibility of the oxidations was applied to the reductions. For the reductions the measured value for **2a** is only 25 mV cathodic from that reported by Hoijtink[36] when corrected for the difference in the reference electrode used. The reduction potentials did not show any obvious trends between substituents, although the actual values did change over a modest potential range within each series. The LUMO energies were all tightly bunched within each series, which is consistent with the observations that the LUMO's had nodes at the sites of substitution.

Conclusions

The results and structural analysis presented lead to a better understanding of CPAH with sterically constrained substituents. Intramolecular HAEs are observed for bromophenyl substituents

(35) Pysh, E. S.; Yang, N. C. *J. Am. Chem. Soc.* **1963**, *85*, 2124.

(36) Hoijtink, G. J. *Recl. Trav. Chim.* **1952**, *71*, 1089–1103.

attached to a central CPAH core, and the magnitude of the effect is proportional to the degree of conjugative overlap possible. The compounds studied comprise a well-defined series where, as shown by structural analysis, the possibility for conjugative overlap goes from near 0 (**1b**) to essentially coplanar (**3**). The molecular mechanics and semiempirical calculations were in agreement with these results. The electrochemical oxidations indicate a small but significant inductive effect for the substituents studied. The reductions likewise showed a modest inductive effect, although the spread in the values observed was large compared to the trends seen.

Acknowledgment. The Midwest Center for Mass Spectroscopy partially funded by the National Science Foundation, Biology DIR 9017262, supplied the high-resolution spectra. The National Science Foundation through Grants CHE-8922685 and CHE-9224324 and the Camille and Henry Dreyfus Foundation gave partial support for the research.